



Full length article

A microfabricated platform with hydrogel arrays for 3D mechanical stimulation of cells [☆]



Haijiao Liu ^{a,b}, Jenna Usprech ^b, Yu Sun ^{a,b,*}, Craig A. Simmons ^{a,b,*}

^a Department of Mechanical and Industrial Engineering, University of Toronto, Toronto M5S 3G8, Canada

^b Institute of Biomaterials and Biomedical Engineering, University of Toronto, Toronto M5S 3G9, Canada

ARTICLE INFO

Article history:

Received 14 July 2015

Received in revised form 15 October 2015

Accepted 25 November 2015

Available online 29 November 2015

Keywords:

Microdevice

Mechanical stimulation

Three-dimensional

Hydrogel

Mesenchymal stromal cell

ABSTRACT

Cellular microenvironments present cells with multiple stimuli, including not only soluble biochemical and insoluble matrix cues but also mechanical factors. Biomaterial array platforms have been used to combinatorially and efficiently probe and define two-dimensional (2D) and 3D microenvironmental cues to guide cell functions for tissue engineering applications. However, there are few examples of array platforms that include dynamic mechanical forces, particularly to enable stretching of 3D cell-seeded biomaterials, which is relevant to engineering connective and cardiovascular tissues. Here we present a deformable membrane platform that enables 3D dynamic mechanical stretch of arrayed biomaterial constructs. Cell-seeded polyethylene glycol norbornene (PEG-NB) hydrogels were bound to miniaturized deformable membranes via a thiol-ene reaction with off-stoichiometry thiol-ene based polydimethylsiloxane (OSTE-PDMS) as the membrane material. Bonding to OSTE-PDMS enabled the 3D hydrogel microconstructs to be cyclically deformed and stretched by the membrane. As a first demonstration, human mesenchymal stromal cells (MSCs) embedded in PEG-NB were stretched for several days. They were found to be viable, spread in the 3D hydrogels, and exhibited a contractile myofibroblast phenotype when exposed to dynamic 3D mechanical deformation. This platform, which is readily scalable to larger arrays, enables systematic interrogation of the relationships between combinations of 3D mechanobiological cues and cellular responses, and thus has the potential to identify strategies to predictably control the construction of functional engineered tissues.

Statement of significance

Current high-throughput biomaterial screening approaches fail to consider the effects of dynamic mechanical stimulation, despite its importance in a wide variety of regenerative medicine applications. To meet this need, we developed a deformable membrane platform that enables 3D dynamic stretch of arrayed biomaterial constructs. Our approach combines microtechnologies fabricated with off-stoichiometry thiol-ene based polydimethylsiloxane membranes that can covalently bond cell-seeded polyethylene glycol norbornene 3D hydrogels, a model biomaterial with tunable adhesive, elastic and degradation characteristics. As a first demonstration, we show that human mesenchymal stromal cells embedded in hydrogels and subjected to dynamic mechanical stimulation undergo myofibroblast differentiation. This system is readily scaled up to larger arrays, and will enable systematic and efficient screening of combinations of 3D mechanobiological and biomaterial cues on cell fate and function.

© 2015 Acta Materialia Inc. Published by Elsevier Ltd. All rights reserved.

[☆] Part of the High Throughput Approaches to Screening Biomaterials Special Issue, edited by Kristopher Kilian and Prabhakar Moghe.

* Corresponding authors at: Department of Mechanical and Industrial Engineering, University of Toronto, Toronto M5S 3G8, Canada.

E-mail addresses: sun@mie.utoronto.ca (Y. Sun), simmons@mie.utoronto.ca (C.A. Simmons).

1. Introduction

Many cells are constantly exposed to mechanical stimuli *in vivo*. Examples include mechanical compression of chondrocytes in cartilage, shear stress on endothelial cells in blood vessels and osteocytes in bone, and cyclic stretching of cardiomyocytes and valvular interstitial cells in the heart. Cells are exquisitely mechanosensitive [1–4], with physical cues playing a vital role in homeostasis

and development at both cellular and tissue levels *in vivo* [2,5,6]. Cell mechanosensitivity is also exploited in regenerative medicine and tissue engineering to induce tissue growth and maturation, often *in vitro* using bioreactors [7,8].

While biomechanical stimuli are potent regulators of cell fate and function, cell responses represent the integration of multiple microenvironmental stimuli, including not only mechanical factors, but also biochemical stimuli, substrate cues, and cell–cell interactions [9,10]. Indeed, cell responses to one type of stimulus can be modulated by other microenvironmental cues, resulting in context-specific responses. For example, the ability for transforming growth factor (TGF)- β 1 to induce myofibroblast differentiation of aortic valve interstitial cells is matrix stiffness-dependent [11] and the mitogenic response of vascular smooth muscle cells to mechanical strain depends on the matrix protein to which the cells are adhered [12].

The complexity of the interactions between multiple microenvironmental cues, and the desire to engineer systems that predictably guide cell function, has led to the development of biomaterial array platforms in which many components of the cellular microenvironment can be prescribed and probed combinatorially to systematically define cue–response relationships [13,14]. Array-based platforms to systematically probe cell responses have mostly used two-dimensional (2D) substrates with defined mechanical, biochemical and topographical properties [15–17]. More recently, arrays of hydrogels with embedded cells have been used to probe responses in 3D [18,19], which is relevant to many physiological scenarios and tissue engineering applications. Synthetic hydrogels with tunable adhesive, biochemical, and mechanical properties are often used in these systems, as they can enable systematic screening of 3D microenvironment factors.

While biomaterial array systems provide new insights into the complexities of microenvironmental regulation, there are few examples of platforms that include mechanical stimuli, despite their emergence as critical regulators of cell and tissue function. To address this need, we and others have developed microfabricated platforms that apply 2D dynamic mechanical stretch to cells adhered to arrays of deformable elastomeric membranes [20–23]. In our platforms, the membranes are actuated by air pressure that is delivered through an underlying channel network [20,24]. The magnitude, frequency, and duty cycle of membrane deflection can be controlled over wide ranges by varying the driving pressure waveform and device dimensions (e.g., membrane size or thickness). Using arrays of deformable membranes, we have probed the mechanobiological responses of cells to combinations of 2D dynamic mechanical stretch, matrix proteins and growth factors with greater throughput than is practical with standard cell stretching systems [20]. Performing similar systematic, combinatorial experiments in 3D environments is also of broad interest. We have adapted our deformable membrane arrays to enable simple hydrogel compression [24,25]. However, for tissues such as heart muscle, heart valves, blood vessels, bladder, and others, more complex 3D loading that includes in-plane tension is likely required for tissue growth *in vitro* [26–30]. There exist several platforms for 3D mechanical stretching of cells (e.g., [27,28,31,32]), but they have low throughput and/or limited capacity to investigate the combined effects of multiple microenvironmental cues on cell functions.

To address this need, we report here a deformable membrane platform that enables dynamic 3D mechanical stretching of arrays of cell-seeded hydrogels. We used polyethylene glycol norbornene (PEG-NB) as a model biomaterial because its adhesion peptide identities and densities, elasticity, and degradability can be tuned precisely and independently, and PEG-NB has been used successfully in biomaterial arrays [19,33]. To address the challenge of applying stretching forces to soft hydrogels [34,35], we used

off-stoichiometry thiol-ene based polydimethylsiloxane (OSTE-PDMS) [39] instead of standard PDMS (i.e., Sylgard 184) as the membrane material, which enabled the PEG-NB hydrogels to be covalently bound to the membrane via a thiol-ene reaction. We demonstrate that membrane actuation causes hydrogel deformation and promotes myofibroblastic differentiation of embedded human bone marrow-derived mesenchymal stromal cells (MSCs). This system can be scaled up to include other microenvironmental cues, and therefore should enable systematic interrogation of the combinatorial effects of a broad range of mechanobiological factors on cell responses and tissue formation *in vitro*.

2. Materials and methods

2.1. Off-stoichiometry thiol-ene based polydimethylsiloxane (OSTE-PDMS)

The formulations of OSTE-PDMS used in this work were based on commercially, readily available, and non-toxic polymers. Dimethylsiloxane copolymer with 4–6% (mercaptopropyl)methylsiloxane or thiol-functionalized PDMS (SMS-042), 4–5% vinylmethylsiloxane or vinyl-functionalized PDMS (VDT-431), and vinyl-terminated PDMS (DMS-V31, DMS-V35 and DMS-V41 with viscosities of 1000, 5000 and 10,000 cSt, respectively) were obtained from Gelest, USA (Fig. 1A). To polymerize thick OSTE-PDMS slabs, we used the photobleaching Irgacure TPO-L from BASF as a photoinitiator. The prepolymer formulations were mixed in predetermined composition ratios (reported as the ratio of thiol-functionalized PDMS:vinyl-functionalized PDMS:vinyl-terminated PDMS of 1000 cSt:vinyl-terminated PDMS of 5000 cSt:vinyl-terminated PDMS of 10,000 cSt in grams), and then degassed in a desiccator and irradiated with a standard table-top UV-lamp (equipped with a 365 nm band pass filter, Omnicure, Canada) for 2 min at an average dose of 6.3 mW/cm². We mixed a series of different composition ratios of the same polymer system to demonstrate the mechanical tuning capability.

OSTE-PDMS is formed by crosslinking the siloxane chains of the polymer components via a thiol-ene reaction (Fig. 1A) [36]. The thiol-containing PDMS and vinyl-containing PDMS polymers are of the same type as standard PDMS, with the only difference being the functional groups. In contrast to standard PDMS, OSTE-PDMS with excess unreacted thiol groups (thus off-stoichiometric) on the surface and in the bulk material can bind PEG-NB hydrogels with excess norbornene groups via the same thiol-ene chemistry (Fig. 2B).

2.2. Compression and tensile testing of OSTE-PDMS

The compressive and tensile moduli of OSTE-PDMS samples were characterized as a function of the varying composition ratios using a commercial mechanical test machine (TestResources 840 series). The compressive moduli were determined from unconfined compression tests. Cylindrical samples (approximately 6 mm in diameter and 5 mm in height) were cut from OSTE-PDMS slabs with three replicates per composition ratio. Each sample was cyclically compressed to 20% strain. Images of samples were taken and analyzed using ImageJ (NIH) to measure the exact sample cross-section areas and initial heights. The compressive modulus was calculated by fitting the corresponding stress–strain curve. For tensile testing, samples were cut into strips of approximately 10 by 30 mm from OSTE-PDMS slabs also with three replicates per composition ratio. Each sample was stretched until rupture. Images before stretching were taken and analyzed using ImageJ to measure the thickness, width and initial length of the strips. The tensile modulus was calculated by fitting the linear portion of the stress–strain curve, which was used as the Young's modulus in the finite

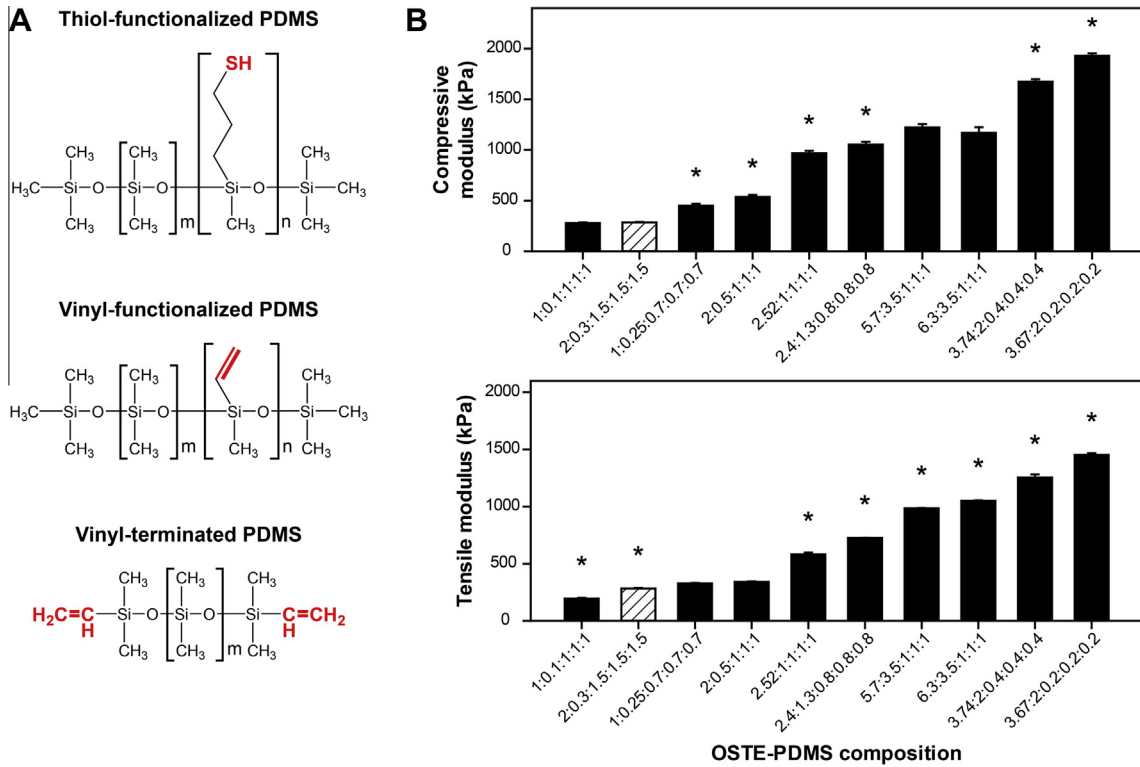


Fig. 1. Off-stoichiometry thiol-ene based polydimethylsiloxane (OSTE-PDMS) components and characterization of compressive and tensile elastic moduli. (A) Three basic PDMS polymers used to formulate the OSTE-PDMS via thiol-ene reaction (noted in red) with the composition ratio given as thiol-functionalized PDMS:vinyl-functionalized PDMS:vinyl-terminated PDMS of 1000 cSt:vinyl-terminated PDMS of 5000 cSt:vinyl-terminated PDMS of 10,000 cSt in grams. (B) The compressive (top) and tensile (bottom) elastic moduli of OSTE-PDMS characterized as a function of different composition ratios. The composition ratio of 2:0.3:1.5:1.5:1.5 (noted with hatched pattern) was selected for demonstration. * $p < 0.05$ versus all other groups; $n = 3$ per group. (For interpretation of the references to color in this figure legend, the reader is referred to the web version of this article.)

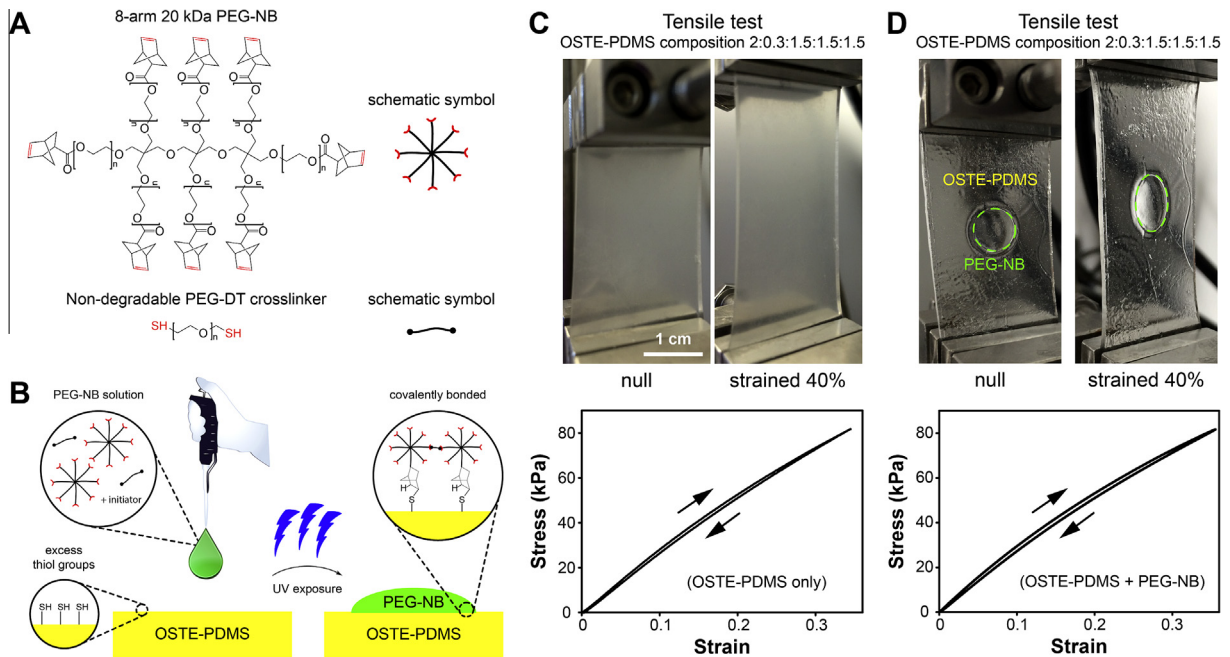


Fig. 2. Demonstration of PEG-NB hydrogel bonding to OSTE-PDMS. (A) 8-arm PEG molecules functionalized with norbornene and dithiolated PEG crosslinker, which is not cell degradable (schematic symbols on the right). (B) Schematic showing polymerization of the PEG-NB hydrogel under UV light with PEG-DT crosslinker bridging PEG-NB molecules into an ordered network, which is also bound to OSTE-PDMS via thiol-ene reaction between norbornene and excess thiol groups from OSTE-PDMS. (C and D) Tensile loading of OSTE-PDMS slab without (C) and with (D) bonded PEG-NB gel.

element analysis to characterize the strain profile of PEG-NB hydrogels under 3D mechanical stretching. The composition ratio of 2:0.3:1.5:1.5:1.5 (thiol-PDMS:vinyl-PDMS:1000 cSt

vinyl-terminated PDMS:5000 cSt vinyl-terminated PDMS:10,000 cSt vinyl-terminated PDMS, in grams) was selected to use for all following tests and experiments.

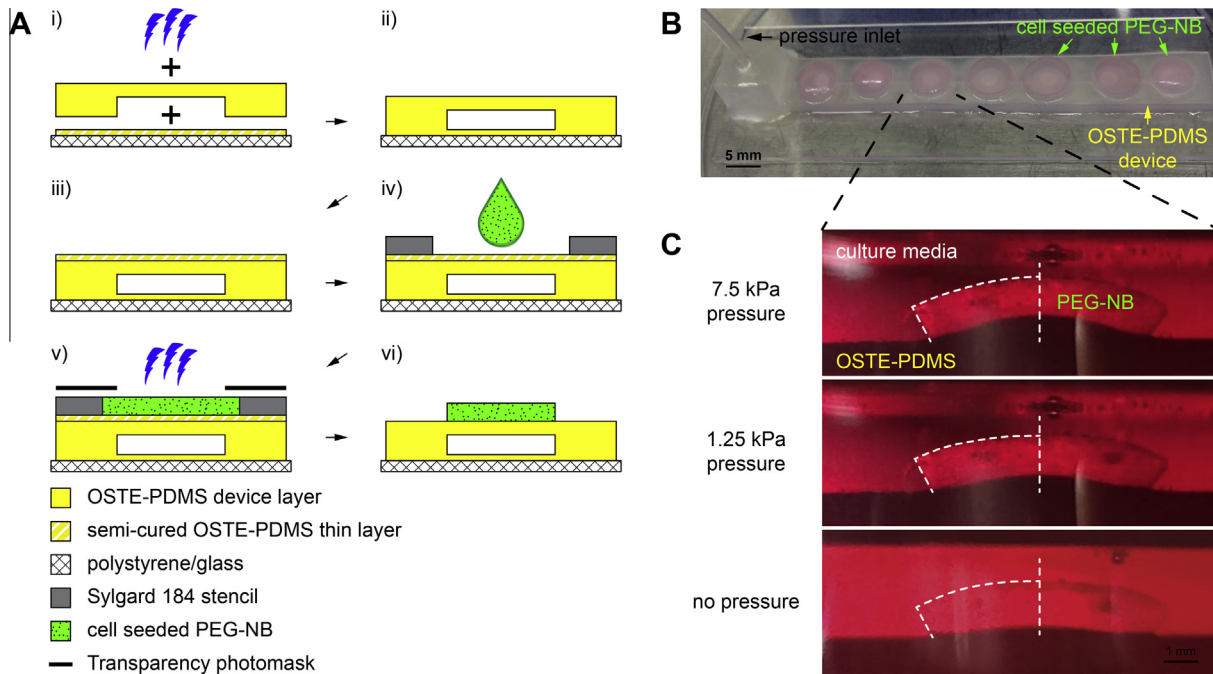


Fig. 3. Integration of PEG-NB hydrogels with OSTE-PDMS deformable membrane devices enables 3D mechanical stretching of PEG-NB hydrogels. (A) Procedures to fabricate the OSTE-PDMS deformable membrane device and integrate and pattern cell-seeded PEG-NB gels with the device. (B) Example of the completed device with hMSCs seeded in the PEG-NB gel array. (C) Side view of a single PEG-NB gel (outlined by white dashed line) in culture media deforming under increasing actuation pressure.

2.3. Poly(ethylene glycol) (PEG) functionalization with norbornene

PEG-norbornene (PEG-NB) was synthesized as previously described [19,33]. Briefly, solid 8-arm PEG-OH (tripentaerythritol core, 20 kDa MW, JenKem, USA), 4-(dimethylamino)pyridine (DMAP, Sigma-Aldrich) and pyridine (Sigma-Aldrich) were dissolved in anhydrous dichloromethane (DCM, Fluka). In a separate round-bottom flask, N,N'-dicyclohexylcarbodiimide (DCC, Fluka) and 5-norbornene-2-carboxylic acid (Sigma-Aldrich) were dissolved in anhydrous DCM. Norbornene carboxylic acid was covalently coupled to the PEG-OH through the carboxyl group by combining the PEG solution and norbornene solution and stirring the reaction mixture overnight under anhydrous conditions. Urea was removed from the reaction mixture using a glass fritted funnel and the filtrate was precipitated in ice cold ether (Fisher). The precipitated PEG-NB was collected from a Buchner funnel and dried overnight. To remove excess norbornene carboxylic acid, PEG-NB was dissolved in deionized H₂O, dialyzed in deionized H₂O for three days, and filtered through a 0.45 μm pore-size syringe filter. The aqueous PEG-NB solution was frozen using liquid nitrogen and lyophilized. Functionalization of PEG with norbornene groups was quantified using proton nuclear magnetic resonance spectroscopy (NMR). The percent functionalization of norbornene groups onto PEG-OH arms was 99%, determined by utilizing the norbornene-associated alkene groups located at 5.8–6.2 PPM [33] (Fig. 2A).

2.4. Bonding PEG-NB hydrogel to OSTE-PDMS

Lyophilized PEG-NB was dissolved in 10 mM phosphate buffered saline (1× PBS) to a final concentration of 6% w/v (3 mM) when combined with 0.05% w/v Irgacure 2959 photoinitiator (I2959, BASF) and 14.7 mM of 3.4 kDa PEG-dithiol crosslinker (PEG-DT, Laysan Bio) to achieve 50% of crosslinking density to form the non-degradable PEG-NB hydrogels for experiments without cells involved. The use of 6% w/v of PEG was to create non-degradable PEG-NB for demonstration purposes. The prepolymer solution of PEG-NB hydrogels was added onto semi-cured

OSTE-PDMS (i.e., reacted OSTE-PDMS under UV light for 30 s only) and irradiated with 365 nm UV light for 2 min at an average dose of 6.3 mW/cm² to polymerize the PEG-NB hydrogel and bond it to OSTE-PDMS via the thiol-ene reaction with the excess thiol groups from OSTE-PDMS and the excess norbornene groups from PEG-NB (Fig. 2B). Cyclic tensile tests were performed on both OSTE-PDMS alone and the composite of OSTE-PDMS and PEG-NB for comparison.

2.5. Cell culture

Cryopreserved human bone marrow-derived mesenchymal stromal cells (MSCs) were obtained from the Texas A&M Health Science Center College of Medicine Institute for Regenerative Medicine at Scott & White through a grant from NCR of the NIH, Grant # P40RR017447. Passage 5–6 MSCs and complete culture media containing 79% α-MEM with L-glutamine, 16.7% fetal bovine serum, 3.3% additional L-glutamine and 1% penicillin/streptomycin were used for all experiments.

2.6. Device fabrication and integration of cell seeded PEG-NB hydrogels

The procedures to fabricate the OSTE-PDMS bulging membrane device and to integrate cell seeded PEG-NB hydrogels are illustrated in Fig. 3A. The fabrication of the OSTE-PDMS device was similar to what we previously reported using standard PDMS [24]. Briefly, master molds for the pressure channel network were machined in aluminum. The prepolymer solution of OSTE-PDMS was cast on this structure, degassed, reacted under UV light for 2 min for polymerization, and peeled off. The master was a relief pattern having 8 × 12 cylindrical disk structures connected by channels. The cylindrical disk structures were 5 mm in diameter, 0.25 mm in height and were spaced by 9 mm center-to-center, conforming to the configuration of standard 96-well plates. Channels connecting the cylindrical disks were 0.25 mm in width and 0.25 mm in height. For the results reported here, the 96-element OSTE-PDMS channel and pressure chamber array was cut into

smaller units (1×7 elements). A mortar layer of semi-cured OSTE-PDMS was first applied on the polystyrene or glass substrate. The device layer was then assembled on top of the mortar layer and was bound to the substrate following exposure to UV light for 1 min (Fig. 3A). The finished OSTE-PDMS bulging membrane devices were stored in a desiccator with vacuum and protected from light. The lifetime of free thiol groups on the surface of devices has not been investigated in detail, but PEG-NB hydrogels were bonded to the devices up to a week after fabrication with no noticeable deterioration in performance over this time.

To enhance cell adhesion and allow for cell-mediated matrix remodeling, the cell degradable PEG-NB was decorated with CRGDS adhesion peptides (GenScript) and crosslinked using the MMP-degradable peptide sequence KCGGPQGIWGQGCK, which is flanked with thiol-containing cysteine groups (GenScript). MSCs suspended in $1 \times$ PBS were mixed 1:1 with PEG-NB solution, which contained a final concentration of 8% w/v (4 mM) of PEG-NB, 35% crosslinking density (5.6 mM KCGGPQGIWGQGCK), 2.5 mM CRGDS, 0.05% w/v Irgacure 2959 photoinitiator, and 1×10^6 cells/mL. To integrate the cell seeded PEG-NB hydrogels onto the OSTE-PDMS bulging membrane device, a mortar layer of semi-cured OSTE-PDMS was first applied on top of the device (Fig. 3A). Stencils of standard PDMS, containing a single cylindrical opening (6 mm diameter and 1 mm height), were sterilized and aligned on the mortar layer concentrically to the OSTE-PDMS membrane unit. 30 μ L of the cell-laden PEG-NB prepolymer solution was added to each stencil well. Next, a transparency photomask with a 5 mm diameter opening window was assembled onto the PDMS stencil and aligned concentrically to the membrane below. The mixture of PEG-NB solution and cells, together with the semi-cured OSTE-PDMS mortar layer was cured under UV light (365 nm; 6.3 mW/cm²) for 2 min. The uncured mixture of PEG-NB with cells was washed away with $1 \times$ PBS. Finally, the PDMS stencils were peeled off, leaving the cell seeded PEG-NB hydrogels covalently bound to the OSTE-PDMS membrane (as shown in Fig. 3A and B). The cell-seeded hydrogel arrays were cultured in complete culture media in a 100 mm Petri dish and maintained in a humidified 37 °C incubator with 5% CO₂. For each experiment, two devices with integrated cell seeded hydrogel arrays were employed. One device was dedicated for 3D mechanical stimulation and the other as a paired static control without mechanical stimulation. Media for both devices was changed every two days.

2.7. Operation of 3D mechanical stretching platform

A diaphragm pump (Shwarzer, model SP 500EC) and a programmable pressure regulator (Marsh Bellofram, model 3410) were used to deliver pressure, P , into the device channel through a single inlet (Fig. 3B). In-house electronics and LabView scripts were built to regulate and monitor pressure. 3D dynamic mechanical stretching of cell seeded PEG-NB hydrogel arrays was performed by applying time-dependent pressure. The pressure was first ramped up to offset $P = 3.75$ kPa and then the sinusoidal P variations (peak-to-peak $P = 7.5$ kPa) were cyclically applied at a frequency of $f = 0.8$ Hz. The PEG-NB hydrogel array in the device dedicated for 3D mechanical stimulation was statically cultured for one day to allow for swelling to equilibrium and then cyclically stretched for 4.5 days. The 3D stretching experiments were repeated three times.

2.8. Characterization of strain profile in PEG-NB and performance of 3D stretching platform

Finite element analysis (FEA) was employed to characterize the strain profile in PEG-NB hydrogels under 3D stretching using ANSYS (V14.0). Non-degradable PEG-NB gels crosslinked with

PEG-DT and without cells were used in these characterization experiments. The non-degradable PEG-NB of 6% w/v had an elastic modulus of 20 kPa, similar to that of 8% w/v degradable PEG-NB used in cell experiments. Hence, mechanical characterization using non-degradable PEG-NB is applicable to the degradable PEG-NB initially. Optical images were taken and analyzed using ImageJ to determine the thickness of the OSTE-PDMS device layer and dimensions of the PEG-NB hydrogel for modeling in ANSYS. The tensile modulus of OSTE-PDMS and elastic modulus of PEG-NB gels as well as the peak pressure applied were used as input data for the FEA model. All materials were assumed to have a Poisson's ratio of 0.49. Images were taken of side views of PEG-NB hydrogels that were experimentally deformed under different pressures and at rest and then analyzed using ImageJ to determine the actual displacement of PEG-NB hydrogels at the top center, which was used to verify the displacement of PEG-NB hydrogels at the top center predicted by FEA.

The strain distribution in the PEG-NB hydrogel under 3D stretching can be tuned by varying the geometry of the gel. As a demonstration, PEG-NB hydrogels with cylindrical and half-elliptical geometries were integrated on the same device array and were deformed with increasing pressure. The cylindrical gel was formed as described above with PDMS stencil. The half-elliptical gel was formed by directly adding a droplet of prepolymer solution of PEG-NB on top of OSTE-PDMS mortar layer without using stencil.

To determine the effects of material fatigue on OSTE-PDMS and PEG-NB, the OSTE-PDMS device array was cyclically stretched with and without PEG-NB gels at 0.8 Hz for 50,000 cycles and the strain profiles under peak pressure were determined. Maximum equivalent strains in each tested unit were normalized to their initial values for comparison.

2.9. Live/Dead staining

Cell viability experiments were performed one day and 5.5 days post seeding. The PEG-NB gels assigned for a viability assay were taken off devices of both static control and 3D mechanical stimulation by cutting along the gel bottom using tweezers. The gels were transferred to a 24-well plate. The gels were then washed with $1 \times$ PBS and stained with 4 μ M calcein-AM and 5 μ M ethidium homodimer-1 (Invitrogen) for 30 min at 37 °C. After staining, the gels were washed again with $1 \times$ PBS and imaged immediately with confocal microscopy. Viability was quantified by dividing the number of live cells over total number of cells.

2.10. F-actin and α -SMA immunostaining

To assess the effect of 3D mechanical stimulation on cell responses, MSCs embedded in PEG-NB hydrogels were co-stained for filamentous actin (F-actin) and α -smooth muscle actin (α -SMA) after 4.5 days of culture (3.5 days of mechanical stimulation), as before [4,37]. The neo-expression and incorporation of α -SMA into stress fibers is considered to be the defining characteristic of differentiated myofibroblast [38], and thus single cell immunofluorescence-based analysis is the most appropriate assay to identify the proportion of functional myofibroblast in a population of cells. The PEG-NB gels assigned for immunostaining were taken off the devices and washed with $1 \times$ PBS. The gels were fixed with 10% neutral buffered formalin and permeabilized with 0.1% Triton X-100. Following fixation, gels were incubated with 3% bovine serum albumin (BSA) in PBS for 20 min and were co-stained for F-actin (phalloidin, 1:50 dilution) and α -SMA (Cy3-conjugated monoclonal mouse anti-human α -SMA clone 1A4, 1 mg/mL, 1:100 dilution), followed by nuclear staining with Hoechst dye (33258, 1:50 dilution) overnight. The gels with

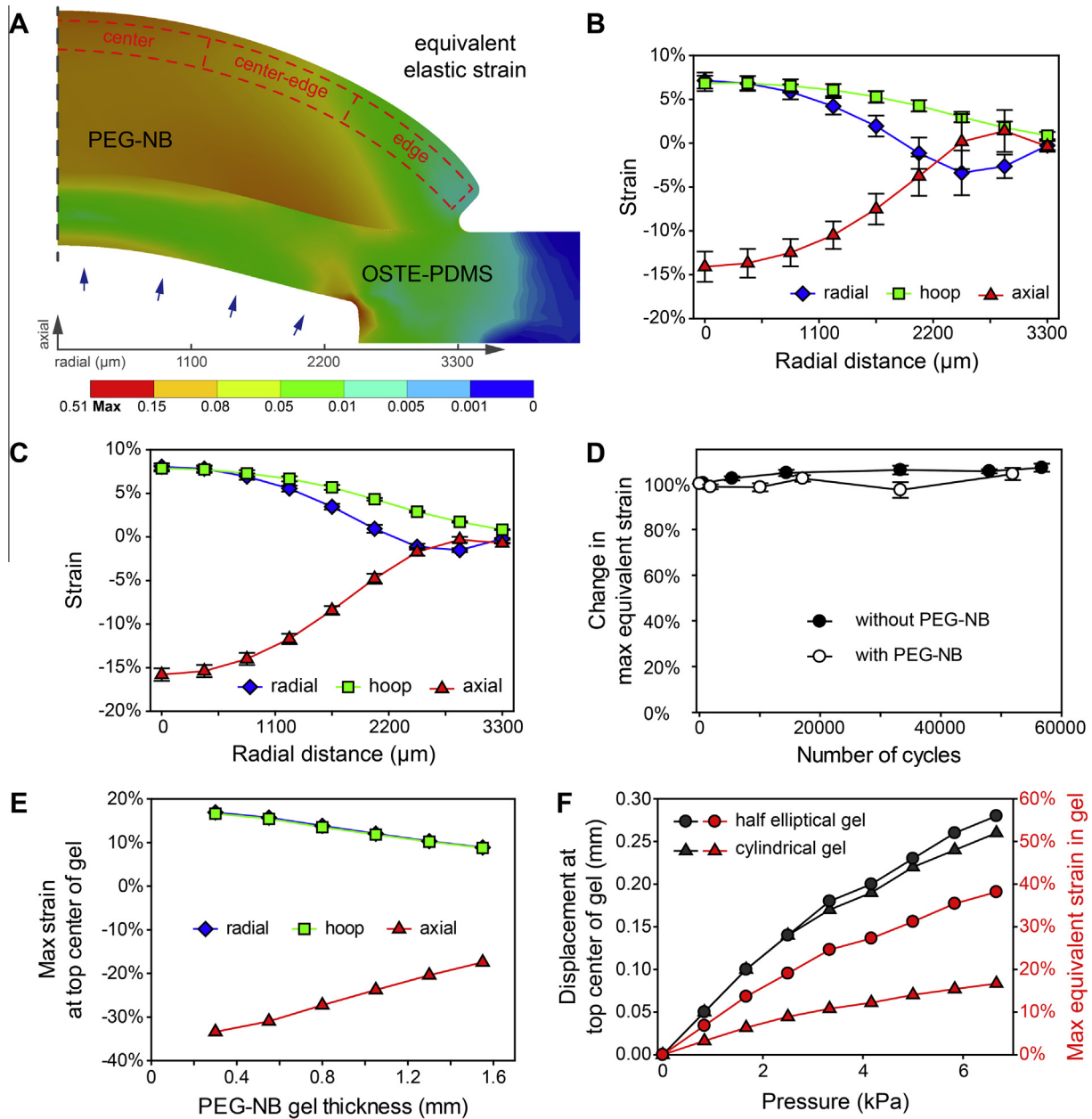


Fig. 4. FEA characterization of the strain profile of PEG-NB gels under 3D stretching. (A) The axisymmetric cross section view of equivalent elastic strain distribution in PEG-NB gels bound to OSTE-PDMS membranes under peak pressure. (B and C) Elastic strain components as functions of radial distance averaged throughout the gel thickness (B) and averaged only in the outlined region (50–250 μm below surface; noted by red dashed line) (C). Plotted values of strains represent the mean and standard deviation of strain values through the thickness. (D) Maximum strain values normalized to their initial values in the OSTE-PDMS membrane alone ($n = 6$) and in the PEG-NB gel ($n = 5$) after more than 50,000 cycles of actuation. (E) FEA predictions for maximum strain magnitudes as a function of gel thickness. (F) Measured displacement of the gel at its center and its corresponding maximum strain as a function of actuation pressure for two different gel geometries.

stained cells were washed and soaked in $1\times$ PBS overnight and imaged with confocal microscopy.

2.11. Confocal microscopy imaging and image analysis

Z-stack images of stained MSCs were acquired with a laser scanning confocal microscope (Nikon A1) using $10\times$ objective (CFI Plan Apo λ $10\times/0.45$, Nikon) [39]. Each PEG-NB gel was mapped to obtain at least 12 independent stacks of images with at least 4 independent stacks for each region (outlined with red dashed line in Fig. 4A). For imaging of cell viability, the PEG-NB gels were imaged from both top and bottom sides. Only images obtained at 50 μm below the surface of gel were analyzed to avoid confounding effects from cells at the 2D surface. Using ImageJ the z-stack

images were divided to individual channels of live and dead cells. Stacked images in each channel were then projected to a single image. The single image was thresholded to generate a mask of cells that was applied back to the single image for counting the number of cells in both channels. The cell viability of each stack was determined as the number of live cells over total number of cells. The cell viability of each individual gel was determined as the average of all stacks from the gel. For imaging of cells stained for F-actin and α -SMA, the PEG-NB gels were imaged only from the top side and only images obtained between 50 and 250 μm below the surface of gel (regions outlined in Fig. 4A) were analyzed to exclude cells at the 2D surface. Similarly the z-stack images were divided to individual channels of nucleus, F-actin and α -SMA using ImageJ and an identical thresholding routine was

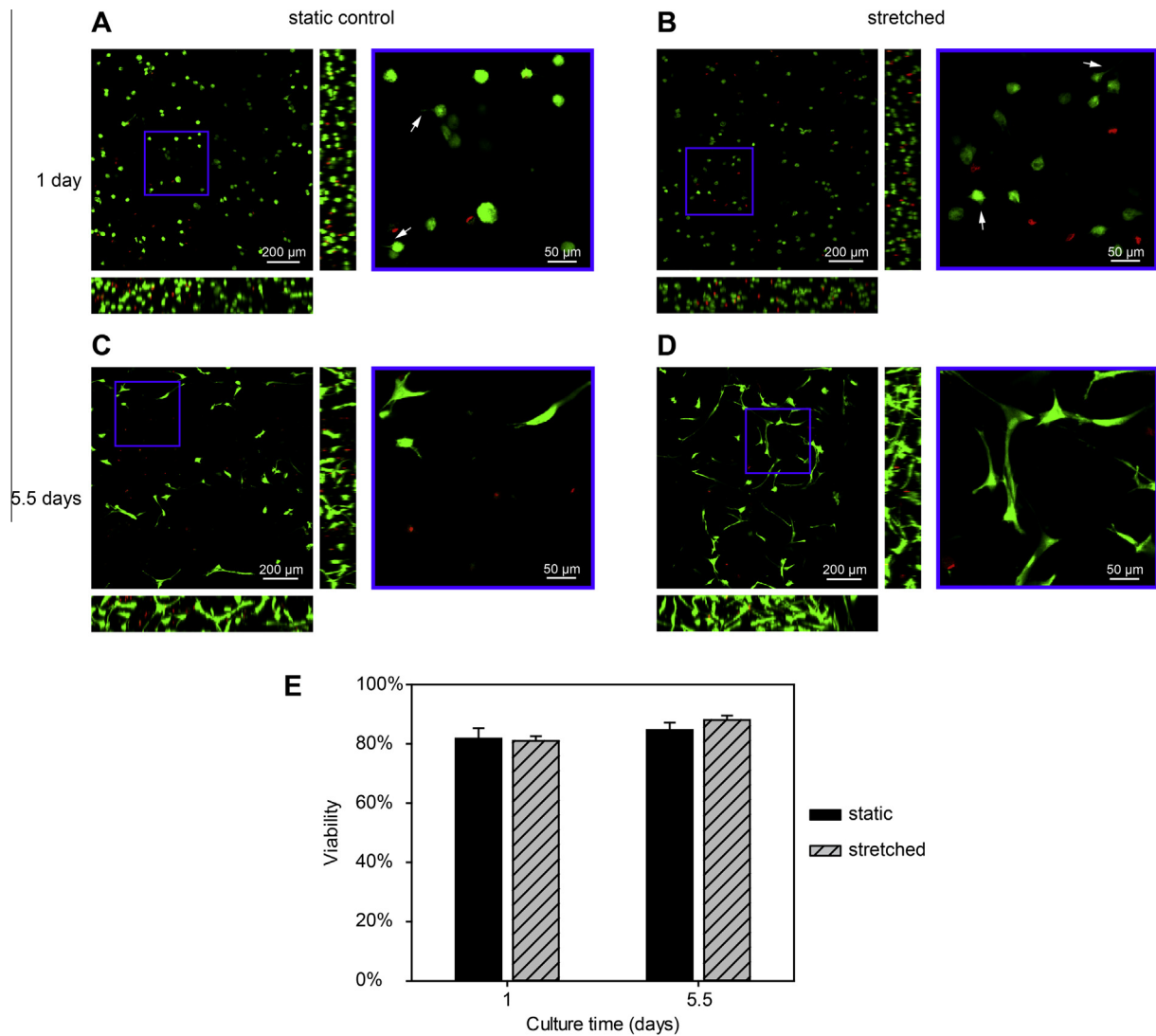


Fig. 5. Characterization of cell viability. (A–D) Representative confocal images of Live/Dead (calcein AM/ethidium homodimer) staining of MSCs (A) in static control gels after 1 day of culture; (B) in gels mounted on the 3D stretching device and culture for 1 day under static conditions, prior to mechanical stimulation; (C) in static control gels after 5.5 days of culture; and (D) in gels cultured on the device for 1 day under static conditions and then subjected to 3D stretching for 4.5 days. Peripheral images are side-view projections. Images on the right of each panel are higher power views of selected cells. Green = living cells; red = dead cells. (E) More than 80% of MSCs were viable at all time points for both static control ($n = 5$ per group) and 3D stretching ($n = 3$ per group) conditions.

applied. The averaged area and integrated density of cellular F-actin and α -SMA were then normalized to those of the nuclei for each stack. The stacks for each region of gel were then averaged based on their subjected 3D nominal tensile strain magnitude for comparison. We used integrated density of fluorescence intensity for comparison between experiments as an objective measure of SMA+ cells.

2.12. Statistical analysis

Statistical analyses were performed using SigmaPlot 13.0. Data are reported as mean \pm standard error of the mean (SEM) unless otherwise noted and were analyzed by one-way and two-way ANOVA with SNK post hoc tests for pairwise comparisons. The mean of measurements for F-actin and α -SMA staining obtained from the static control gels were used to normalize the paired gels subjected to 3D stretching. Hence, results could be compared from different experiments, where variability in the control values occurred. The control value of $1 \pm$ SEM in Fig. 7D represents the mean of all normalized control values from three repeated

experiments. The statistical significance in each comparison was evaluated with $p \leq 0.05$.

3. Results

3.1. Formation of an OSTE-PDMS and PEG-NB composite material

OSTE-PDMS after crosslinking, as shown in Fig. 1B and Fig. 2C and D, is an elastomeric polymer with a lower but comparable modulus to that of the standard Sylgard 184 PDMS. Like standard PDMS, its mechanical properties are also tunable. The compressive and tensile moduli of OSTE-PDMS increased from 278 ± 8 kPa to 1929 ± 25 kPa (Fig. 1B top), and from 196 ± 5 kPa to 1453 ± 15 kPa (Fig. 1B bottom), respectively, when the ratio of vinyl-functionalized PDMS to vinyl-terminated PDMS was increased from 0.1 to 10. We selected the OSTE-PDMS composition ratio of 2:0.3:1.5:1.5:1.5 for subsequent experiments, as this ratio produces OSTE-PDMS that is deformable, yet strong enough for handling during device fabrication. Importantly, this ratio also has a higher ratio of excess thiol groups than other composition

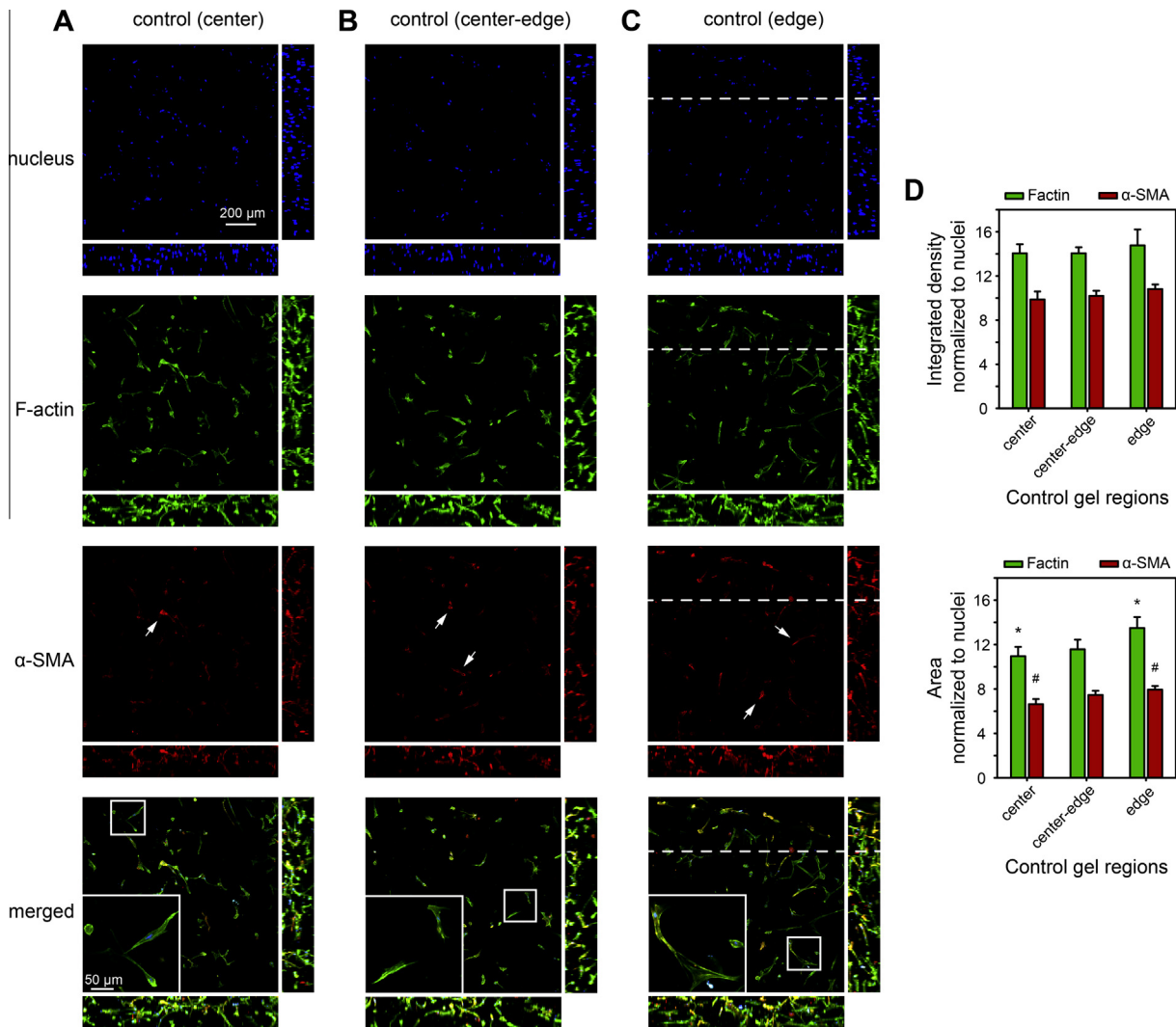


Fig. 6. Cell responses under static culture. (A–C) Representative confocal images of immunostaining of MSCs for filamentous actin (F-actin), α -smooth muscle actin (α -SMA) and nuclei at the (A) center, (B) center-edge and (C) edge regions of the gel (arrows indicate cells with positive staining of α -SMA; dashed line denotes 50 μ m into the surface of gel). (D) Quantities of integrated density of fluorescent intensity (top) and projected area (bottom), both normalized to nucleus, were used to characterize cell responses in each region of the gel for both F-actin ($n = 5$ per group) and α -SMA ($n = 5$ per group). * and # indicate statistically significant differences ($p < 0.05$) between groups with the symbols.

ratios to enable strong bonding to PEG-NB gels. Cyclic tensile stretching of the OSTE-PDMS slab with and without an attached PEG-NB hydrogel showed similar tensile loading behavior with negligible hysteresis (Fig. 2C and D). The PEG-NB gel remained attached to and was deformed elastically with the OSTE-PDMS slab. For the OSTE-PDMS and PEG-NB composite demonstrated here, strong bonding to the PEG-NB gel resisted up to 40% of uniaxial strain during macroscale stretching (Fig. 2D).

3.2. 3D stretching of PEG-NB hydrogels

Fig. 3B shows an example of arrayed PEG-NB hydrogels with encapsulated MSCs, covalently bound to the OSTE-PDMS membrane device. After 4.5 days of 3D mechanical stimulation, no detachment of PEG-NB gels was observed for any experiment. While we have not specifically tested the maximum strain that will delaminate the PEG-NB gel from the OSTE-PDMS membrane device, 40% tensile strain is a conservative estimate. Fig. 3C and the Supplemental Movie show the side view of a single PEG-NB gel in culture media with different actuation pressures applied. The OSTE-PDMS membrane below the PEG-NB gel was increasingly

bulged up (black region) with increasing pressure from 0 to 1.25 kPa to 7.5 kPa. As a result, the PEG-NB gel also bulged up and the center of the top of gel was significantly displaced upwards (outlined in white dashed line) with the edges of the gel remaining almost unchanged, indicating that the PEG-NB gel was deformed and stretched.

FEA modeling was conducted to characterize the maximum local strain generated in the PEG-NB gel under 3D mechanical stimulation. The FEA results shown in Fig. 4A depict an equivalent elastic strain field of the axisymmetric model, simulating the PEG-NB gel bound to the OSTE-PDMS bulging membrane under a peak pressure. The peak gel displacements measured experimentally were $98 \pm 2\%$ and $100 \pm 1\%$ of those predicted by FEA for 5.8 kPa and 7.5 kPa actuation pressures, respectively, validating the FEA predictions for gel deformation. The results of the FEA showed that the equivalent strains were relatively uniform in the central portion of the PEG-NB gel and became more heterogeneous towards the radial edge (Fig. 4A). Fig. 4B shows the mean strain and variation of the strain components throughout the gel thickness (standard deviation represented by error bars) along the radial, circumferential (hoop) and axial direction, as a function of radial

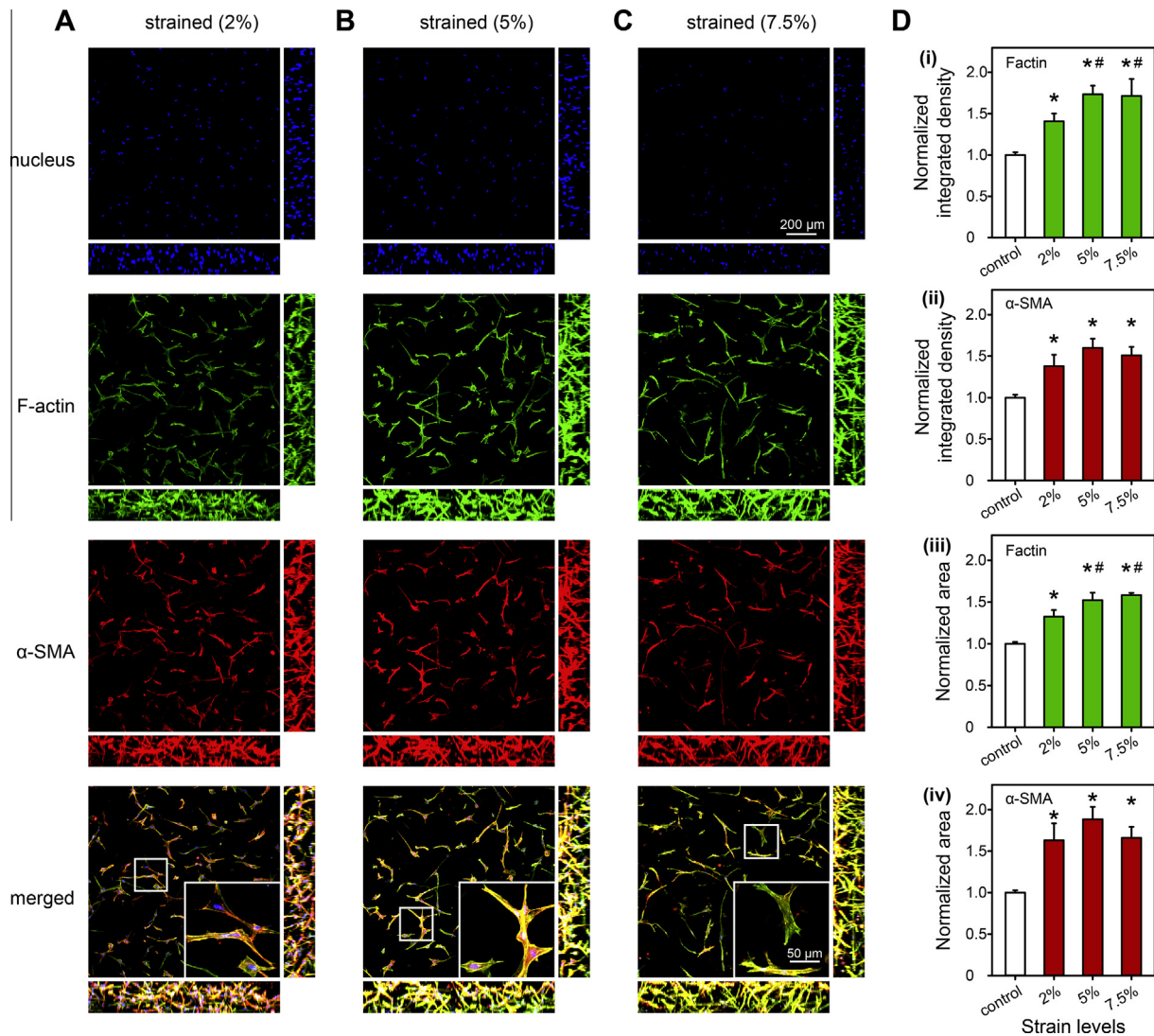


Fig. 7. Contractile phenotype of MSCs with 3D mechanical stretching. (A–C) Representative confocal images of immunostaining of MSCs for F-actin, α -SMA and nuclei subjected to nominal tensile strain of (A) 2%, (B) 5% and (C) 7.5%. (D) The integrated density (i and ii) and projected area (iii and iv) of cells for F-actin and α -SMA are normalized to the static control for comparison. MSCs subjected to 3D stretching are significantly more spread and have significantly higher levels of F-actin and α -SMA expression. * indicates statistically significant differences ($p < 0.05$) relative to the control and # indicates significant differences ($p < 0.1$) relative to the 2% strain group. $n = 3$ for the 7.5% strain group, $n = 6$ for all other groups.

distance in PEG-NB gel. The gel experiences tensile radial and hoop strains that are maximal and comparable in magnitude in the center region and decrease radially. Similarly, the compressive axial strain is maximal at the center and decreases radially. The radial and axial strain components vary modestly through the thickness of the gel; in contrast, the hoop strain is relatively constant through the gel thickness. In regions close to the gel surface (as outlined in Fig. 4A), there is negligible variation in the axial direction, and the variations of the gel strain components are largely dependent on the radial position only (Fig. 4C). Importantly, during long-term, continuous actuation, the relative change in maximum equivalent strain in the OSTE-PDMS membrane (without PEG-NB) and in the PEG-NB gel was less than 10% (Fig. 4D), with no significant difference in the maximum strain in gels after more than 50,000 actuation cycles ($p = 0.21$). Thus, the system provides consistent strain application to the gels during long-term actuation.

In addition to varying the applied pressure, the strains applied to cells in the adhered gels can be tuned by varying the gel dimensions and geometry. For example, by reducing the gel thickness from 1.6 mm to 0.3 mm, the maximum tensile strain in the gel

increases from 8.9% to 17% (Fig. 4E). Additionally, changing the gel geometry alters the strain magnitudes and distribution in the gel. For example, cylindrical and half-elliptical shaped gels both displace similarly for a given pressure (Fig. 4F), but exhibit very different strain profiles (Fig. S1) and maximum equivalent strains (Fig. 4F).

3.3. Viability of MSCs in 3D PEG-NB gels

We observed MSC viability in PEG-NB gels for both static control and 3D mechanical stimulated conditions. Fig. 5A and B show representative images along with cross section projections of Live/Dead staining of MSCs after one day of culture in the devices for static control (Fig. 5A) and mechanical stimulation (Fig. 5B, before stretching) conditions. The majority of cells at this point were living and remained mostly spherical in shape for both conditions. Some cells appeared to be spreading with visible filopodial protrusions (arrows in Fig. 5A and B). The cell viability rate throughout the PEG-NB gel at this point was $81.8 \pm 2.6\%$ for static control and $81 \pm 3.3\%$ for 3D mechanical stimulation (Fig. 5E).

Fig. 5C and D show Live/Dead staining of MSCs after 5.5 days of culture for static control (Fig. 5C) and mechanical stimulation (Fig. 5D, 4.5 days of stretching) conditions. Most cells by this time were still living and well spread for both conditions. The cell viability rate throughout the gel was $84.7 \pm 2.6\%$ for static control and $88 \pm 3.3\%$ for the mechanically stimulated group (Fig. 5E). There were no significant differences in cell viability between different culture periods ($p = 0.12$) and between static control and 3D mechanical stimulation conditions ($p = 0.68$).

3.4. Myofibrogenic response of MSCs to 3D mechanical stimulation

To observe the phenotypic differences of MSCs in response to 3D dynamic mechanical stretching, we co-stained the cells for expression of F-actin and α -SMA, the latter being a marker of myofibroblast differentiation [38]. We considered expression in three regions of the gel (center, center-edge, and edge, as indicated in Fig. 4A), representing regions with nominal average tensile strains of 7.5%, 5%, and 2%, respectively. Fig. 6 shows representative images of immunostaining of F-actin and α -SMA as well as nuclei of MSCs in static control PEG-NB gels after 4.5 days of culture for different regions. Most cells were well spread based on the F-actin staining (Fig. 6A–C), with no significant differences in the normalized integrated density of F-actin ($p = 0.86$) among different regions of the gel (Fig. 6D). Normalized α -SMA expression was marginally significantly different between the edge and center regions ($p = 0.06$), but the expression levels were overall low and the differences minor (8.7% difference between edge and center) (Fig. 6A–D). Similarly, the projected area of individual cells for F-actin and α -SMA were significantly different between the center and edge regions ($p = 0.03$ for both), but the differences were minor when compared with those induced by the 3D mechanical stimulation condition, as described below. Both the integrated density and projected area of individual cells normalized to nucleus for F-actin were higher than those for α -SMA, regardless of regions in the gel (Fig. 6D).

Fig. 7 shows representative images of immunostaining of F-actin, α -SMA, and nuclei of MSCs in 3D mechanically stretched gels after 4.5 days of culture (3.5 days of stimulation) for different levels of strain. In comparison with MSCs in static control gels, cells subjected to the 3D mechanical stimulation spread more with long stable edges according to the cellular F-actin staining for all strain magnitude levels (Fig. 7A–C). There were significant differences in the integrated density of cellular F-actin normalized to that of static controls between 3D strained and static control conditions (Fig. 7D (i)), with significantly greater expression in all strained groups relative to the static control ($p < 0.001$) and marginally significantly greater expression in the 5% ($p = 0.06$) and 7.5% ($p = 0.08$) regions relative to the 2% region. Similarly, the projected area of individual cells based on F-actin staining was greater in all strained conditions vs. the static control ($p < 0.001$) and greater in the 5% ($p = 0.05$) and 7.5% ($p = 0.09$) regions relative to the 2% region (Fig. 7D(iii)).

In comparison with MSCs from static control, more cells stained positively for α -SMA with a larger stained area for all strain magnitudes in the 3D stretched condition (Fig. 7A–C). There were significant differences in the integrated density of α -SMA ($p = 0.004$, Fig. 7D(ii)) and in the projected area of α -SMA ($p = 0.003$, Fig. 7D (iv)) between all 3D strained conditions and static controls, but no significant differences between the different strain levels for α -SMA expression ($p \geq 0.30$) or area ($p > 0.35$).

4. Discussion

Biomaterial array platforms are increasingly used to systematically probe and identify 2D and 3D microenvironmental cues to

control cell functions for specific tissue engineering applications. However, there still exist few array-based platforms that include the capability of dynamic mechanical actuation, particularly to enable 3D stimulation. Here we demonstrated the formation of an OSTE-PDMS and PEG-NB composite material, and the integration of PEG-NB hydrogel array into bulging membrane devices for 3D mechanical stretching of cells. The applicability of the OSTE-PDMS and PEG-NB system to 3D culture of hMSCs was confirmed, and differences in the phenotype of hMSCs with 3D mechanical stretching were observed. Because the system is readily parallelizable and scalable to include other microenvironmental cues, it can enable systematic and efficient screening of the combinatorial effects of dynamic 3D mechanical stimulation, and biomaterial and biochemical cues on cell responses *in vitro*.

We used PEG-NB hydrogels as a model of a biomaterial with tunable mechanical, adhesive, and degradation properties that are relevant to soft connective and cardiovascular tissues. Compared with other PEG systems (e.g., PEG-diacrylate), the faster step growth polymerization of PEG-NB yields higher initial cell viability under UV irradiation [25], a highly ordered and repeatable network [33], and a reduction in the production of radical species, rendering better bioactivity of encapsulated proteins [40]. For the purpose of defining the 3D microenvironment of cells, an attractive feature of PEG-NB hydrogels is the ability to tailor and decouple the hydrogel material and biochemical properties. Material properties such as mechanical stiffness can be tuned by adjusting the PEG content, the molecular weight of PEG monomer, or the extent of crosslinking. Although only one stiffness of the PEG-NB gels was demonstrated here, PEG-NB gels with a range of stiffness (e.g., 0.3–30 kPa of elastic modulus) [19,41] can be integrated in the same manner as described. Cell adhesion can also be tailored by introducing ligand peptide sequences derived from ECM proteins that are covalently bound as pendant groups within the PEG-NB network. Degradability of the gels, important for cell spreading and matrix remodeling, is achieved by crosslinking the gels using MMP-cleavable peptides. These peptides can be replaced with PEG-DT to make gels non-degradable by cells as needed.

Our data show that MSCs thrive with high cell viability (>80%) and spread well within PEG-NB gels under both static control and 3D mechanical stimulation conditions (Fig. 5). We have tested the device under continuous actuation without PEG-NB and with non-degradable PEG-NB (Fig. 4D). There was no significant variation of strain generated in the OSTE-PDMS membrane and in the non-degradable PEG-NB gels during the test period indicating that there are no intrinsic material property changes with the device during experiments. The hydrogels were not expected to undergo substantial cell-induced matrix remodeling during this course of culture [42], and there was no evidence of gel degradation based on optical measurements of gel deformation and finite element analysis during the culture periods examined. However, with longer culture, cell-mediated matrix remodeling would be expected to change the properties of the 3D construct leading to different gel deformation (and strains) under constant pressure. This could be monitored by optical measurement of gel deformation and FEA, as was done here, or alternatively by using integrated strain sensors for continuous on-chip monitoring [24].

Application of complex 3D loading, particularly tensile forces, to soft hydrogels is challenging, particularly at the microscale. The challenge is compounded by the fact that microfabricated devices are typically constructed from Sylgard 184 PDMS, which is inherently hydrophobic and difficult to bond to. Surface treatment of PDMS with a silanizing agent may be used to immobilize biomaterials but the silanization process is relatively complicated and subject to hydrophilic instability similar to that of oxygen plasma treatment for bonding [43]. To overcome these challenges, we incorporated OSTE-PDMS membranes in our microdevice to enable

direct bonding of PEG–NB gels using excess functional thiol groups from OSTE–PDMS. This novel approach provides a stable interface that requires only simple UV curing (Figs. 2 and 3). The whole process of device fabrication and integration of cell seeded PEG–NB gels is relatively simple and can be done with a table top UV lamp without requiring other cleanroom equipment (Fig. 3). The design reported here is based on a 96-well microplate footprint, and the devices can be scaled up to increase throughput. In the current experimental setup, the PEG–NB gels were cultured in the same pool of media (Fig. 3B). If desired, the device can be modified to isolate individual wells using bottomless well plates or other barriers.

The bulging membrane actuation method we applied here induced complex, spatially heterogeneous 3D strain fields in the hydrogels, with both in-plane biaxial tension and through-thickness compression (Fig. 4). This was intended since this deformation mode is relevant to many tissues of interest (e.g., blood vessels, heart valves, bladder, etc.), and spatially heterogeneous strain profiles recapitulate the 3D strain field of highly organized structures, such as the heart valve [44]. While the system does not permit precise control over individual strain components, strain levels and distributions can be controlled by varying the actuation pressure and gel dimensions (Fig. 4), and spatial heterogeneity can be addressed by regional image analyses (Figs. 6 and 7).

Nonetheless, coupled 3D strain components and spatial heterogeneity can confound interpretation of cell responses and limit the ability to attribute specific responses to specific mechanical stimuli. Thus, this platform as configured here is best suited as a screening tool to identify “hits” for cells and tissues for which this type of loading is relevant or to generate specific hypotheses that can be tested more comprehensively using other systems that more precisely define the dynamic mechanical environment, but with limited throughput [17]. More generally, the strategy of immobilizing arrays of PEG–NB gels to OSTE–PDMS membranes is generalizable to a variety of mechanical loading modes. For example, the membranes could be deformed under uniaxial or biaxial tension using a traditional stretch bioreactor [45,46] to subject the gels to in-plane tension, with minimal through-thickness compression and precise control over the anisotropy of the strain field.

As a first demonstration of the platform, MSCs were encapsulated in PEG–NB gels on the device and the expression of F-actin and α -SMA were measured as a function of strain application. The cells tolerated the on-device polymerization process well, remaining highly viable and well-spread throughout the culture period (Fig. 5). In static gels, MSC spreading and expression of F-actin and α -SMA were relatively uniform, with minor increases at the gel edge (Fig. 6), possibly due to the rigid boundary condition imposed by the taut membrane. However, compared with the increases in spreading and F-actin and α -SMA expression in response to 3D mechanical strain (Fig. 7), the spatial variations without dynamic loading were negligible. Under 3D strain, the cells were significantly more spread with long stable edges, when compared with cells in static control (Fig. 7). These results are in agreement with previous 2D stretching studies [20,47,48]. Similarly, the dose-dependent increase in F-actin and increase in α -SMA expression with strain (Fig. 7) is consistent with observations of tension-induced myofibroblast differentiation of MSC-like cells in 2D by us [20] and others [47,49]. In other mesenchymal progenitor cells, we have observed threshold responses in mechanically-regulated α -SMA expression, with stepwise increases with increasing mechanical tension [11]. At greater levels of strain, we would expect enhanced myofibroblast differentiation with greater α -SMA expression and production of extracellular matrix proteins like collagen [20,28,47]. However, cellular responses to mechanical stimulation are rarely linear and the optimal combination of mechanical stimulation parameters (strain magnitude, frequency, duty cycle, etc.) is difficult to identify. In

addition, cell adaptation during *in vitro* mechanical conditioning might occur, causing cell unresponsiveness, which can be mitigated by intermittent loading regimes [28]. A miniaturized platform with high-throughput capacity, as is possible with the platform presented here, could be useful to systematically and efficiently screen loading parameters to identify optimal responses. Cell response to mechanical stimulation is also modulated by other microenvironmental cues. In our previous work in 2D [20], stretch-induced α -SMA expression was dependent on the extracellular matrix protein to which the cells were attached; others have reported similar cross-talk between 2D matrix stiffness and dynamic stretch responses [48,50]. Although not demonstrated here, this platform would enable similar investigations of the effects of combined microenvironmental cues on cell functions including myofibroblast differentiation, but in 3D, by prescribing adhesion ligands and/or matrix elasticity of the PEG–NB gels and subjecting them to 3D mechanical stimulation. Furthermore, emerging evidence suggests that mechanoregulation of pluripotent stem cells (PSCs) may be a potent means to complement the effects of soluble cues and enable PSCs to reach their full therapeutic potential [51]. This platform could be used to identify new mechanobiology-based strategies to predictably control MSC/PSC fate and function.

5. Conclusions

PEG–NB hydrogel arrays with encapsulated mesenchymal stromal cells were integrated into a miniaturized bulging OSTE–PDMS membrane platform to enable cyclic 3D mechanical stimulation of hydrogel arrays. hMSCs were viable and well spread within the hydrogels. 3D mechanical stimulation significantly increased MSC spreading and F-actin and α -SMA expression, indicative of myofibroblast differentiation. The platform design is amenable to parallelization and will be useful to systematically and efficiently screen and optimize the combinatorial effects of 3D mechanical stimulation protocols, biomaterial properties, and biochemical stimuli on cell responses and tissue formation *in vitro*.

Acknowledgements

The authors thank Oleg Chebotarev for helpful suggestions and acknowledge financial support from the NSERC CREATE Program in Microfluidic Applications and Training in Cardiovascular Health (MATCH) (H.L.), the Canadian Institutes of Health Research (MOP-130481), and the Canada Research Chairs in Mechanobiology (C.S.) and Micro and Nanoengineering Systems (Y.S.).

Appendix A. Supplementary data

Supplementary data associated with this article can be found, in the online version, at <http://dx.doi.org/10.1016/j.actbio.2015.11.054>.

References

- [1] J.H.-C. Wang, B.P. Thampatty, An introductory review of cell mechanobiology, *Biomech. Model. Mechanobiol.* 5 (2006) 1–16, <http://dx.doi.org/10.1007/s10237-005-0012-z>.
- [2] A.J. Engler, S. Sen, H.L. Sweeney, D.E. Discher, Matrix elasticity directs stem cell lineage specification, *Cell* 126 (2006) 677–689, <http://dx.doi.org/10.1016/j.cell.2006.06.044>.
- [3] J.A. Pedersen, M.A. Swartz, Mechanobiology in the third dimension, *Ann. Biomed. Eng.* 33 (2005) 1469–1490, <http://dx.doi.org/10.1007/s10439-005-8159-4>.
- [4] H. Liu, Y. Sun, C.A. Simmons, Determination of local and global elastic moduli of valve interstitial cells cultured on soft substrates, *J. Biomech.* 46 (2013) 1967–1971, <http://dx.doi.org/10.1016/j.jbiomech.2013.05.001>.

- [5] D.E. Ingber, Mechanical control of tissue morphogenesis during embryological development, *Int. J. Dev. Biol.* 50 (2006) 255–266, <http://dx.doi.org/10.1387/ijdb.052044di>.
- [6] K. Lau, H. Tao, H. Liu, J. Wen, K. Sturgeon, N. Sorfazlian, et al., Anisotropic stress orients remodelling of mammalian limb bud ectoderm, *Nat. Cell Biol.* 17 (2015) 569–579, <http://dx.doi.org/10.1038/ncb3156>.
- [7] J.A. Burdick, G. Vunjak-Novakovic, Engineered microenvironments for controlled stem cell differentiation, *Tissue Eng.* 15 (2009).
- [8] M.S. Sacks, F.J. Schoen, J.E. Mayer, Bioengineering challenges for heart valve tissue engineering, *Annu. Rev. Biomed. Eng.* 11 (2009) 289–313, <http://dx.doi.org/10.1146/annurev-bioeng-061008-124903>.
- [9] D.E. Discher, D.J. Mooney, P.W. Zandstra, Growth factors, matrices, and forces combine and control stem cells, *Science* 324 (2009) 1673–1677, <http://dx.doi.org/10.1126/science.1171643>.
- [10] D. Ingber, Cellular mechanotransduction: putting all the pieces together again, *FASEB J.* (2006) 811–827, <http://dx.doi.org/10.1096/fj.05>.
- [11] J.-H. Chen, W.L.K. Chen, K.L. Sider, C.Y.Y. Yip, C.A. Simmons, β -Catenin mediates mechanically regulated, transforming growth factor- β 1-induced myofibroblast differentiation of aortic valve interstitial cells, *Arterioscler. Thromb. Vasc. Biol.* 31 (2011) 590–597, <http://dx.doi.org/10.1161/ATVBAHA.110.220061>.
- [12] E. Wilson, E. Wilson, K. Sudhir, K. Sudhir, H.E. Ives, H.E. Ives, Mechanical strain of rat vascular smooth muscle cells is sensed by specific extracellular matrix/integrin interactions, *J. Clin. Invest.* 96 (1995) 2364–2372.
- [13] C.J. Flaim, S. Chien, S.N. Bhatia, An extracellular matrix microarray for probing cellular differentiation, *Nat. Methods* 2 (2005) 119–125, <http://dx.doi.org/10.1038/nmeth736>.
- [14] A. Khademhosseini, R. Langer, J. Borenstein, P.J. Vacanti, Microscale technologies for tissue engineering and biology, *Proc. Natl. Acad. Sci.* 103 (2006) 2480–2487, <http://dx.doi.org/10.1073/pnas.0507681102>.
- [15] W.L.K. Chen, M. Likhithpanichkul, A. Ho, C.A. Simmons, Integration of statistical modeling and high-content microscopy to systematically investigate cell-substrate interactions, *Biomaterials* 31 (2010) 2489–2497, <http://dx.doi.org/10.1016/j.biomaterials.2009.12.002>.
- [16] M.L. Yarmush, K.R. King, Living-cell microarrays, *Annu. Rev. Biomed. Eng.* 11 (2009) 235–257, <http://dx.doi.org/10.1146/annurev.bioeng.10.061807.160502>.
- [17] C. Moraes, Y. Sun, C.A. Simmons, (Micro)managing the mechanical microenvironment, *Integr. Biol. (Camb)* 3 (2011) 959–971, <http://dx.doi.org/10.1039/c1ib00056j>.
- [18] A. Dolatshahi-Pirouz, M. Nikkha, A.K. Gaharwar, B. Hashmi, E. Guermani, H. Aliabadi, et al., A combinatorial cell-laden gel microarray for inducing osteogenic differentiation of human mesenchymal stem cells, *Sci. Rep.* 4 (2014) 3896, <http://dx.doi.org/10.1038/srep03896>.
- [19] E.H. Nguyen, M.R. Zanolli, M.P. Schwartz, W.L. Murphy, Differential effects of cell adhesion, modulus and VEGFR-2 inhibition on capillary network formation in synthetic hydrogel arrays, *Biomaterials* 35 (2014) 2149–2161, <http://dx.doi.org/10.1016/j.biomaterials.2013.11.054>.
- [20] C. Moraes, M. Likhithpanichkul, C.J. Lam, B.M. Beca, Y. Sun, C.A. Simmons, Microdevice array-based identification of distinct mechanobiological response profiles in layer-specific valve interstitial cells, *Integr. Biol. (Camb)* 5 (2013) 673–680, <http://dx.doi.org/10.1039/c3ib20254b>.
- [21] Y. Kamotani, T. Bersano-Begley, N. Kato, Y.-C. Tung, D. Huh, J.W. Song, et al., Individually programmable cell stretching microwell arrays actuated by a Braille display, *Biomaterials* 29 (2008) 2646–2655, <http://dx.doi.org/10.1016/j.biomaterials.2008.02.019>.
- [22] C.S. Simmons, J.Y. Sim, P. Baechtold, A. Gonzalez, C. Chung, N. Borghi, et al., Integrated strain array for cellular mechanobiology studies, *J. Micromech. Microeng.* 21 (2011) 054016, <http://dx.doi.org/10.1088/0960-1317/21/5/054016>.
- [23] C.S. Simmons, A.J.S. Ribeiro, B.L. Pruitt, Formation of composite polyacrylamide and silicone substrates for independent control of stiffness and strain, *Lab Chip* 13 (2013) 646–649, <http://dx.doi.org/10.1039/c2lc41110e>.
- [24] L. MacQueen, O. Chebotarev, C.A. Simmons, Y. Sun, Miniaturized platform with on-chip strain sensors for compression testing of arrayed materials, *Lab Chip* 12 (2012) 4178–4184, <http://dx.doi.org/10.1039/c2lc40670e>.
- [25] C. Moraes, G. Wang, Y. Sun, C.A. Simmons, A microfabricated platform for high-throughput unconfined compression of micropatterned biomaterial arrays, *Biomaterials* 31 (2010) 577–584, <http://dx.doi.org/10.1016/j.biomaterials.2009.09.068>.
- [26] K. Tobita, L.J. Liu, A.M. Janczewski, J.P. Tinney, J.M. Nonemaker, S. Augustine, et al., Engineered early embryonic cardiac tissue retains proliferative and contractile properties of developing embryonic myocardium, *Am. J. Physiol. Heart Circ. Physiol.* 291 (2006) H1829–H1837, <http://dx.doi.org/10.1152/ajpheart.00205.2006>.
- [27] W.-H. Zimmermann, Tissue engineering of a differentiated cardiac muscle construct, *Circ. Res.* 90 (2001) 223–230, <http://dx.doi.org/10.1161/hh0202.103644>.
- [28] Z.H. Syedain, J.S. Weinberg, R.T. Tranquillo, Cyclic distension of fibrin-based tissue constructs: evidence of adaptation during growth of engineered connective tissue, *Proc. Natl. Acad. Sci. U.S.A.* 105 (2008) 6537–6542, <http://dx.doi.org/10.1073/pnas.0711217105>.
- [29] Z.H. Syedain, R.T. Tranquillo, Controlled cyclic stretch bioreactor for tissue-engineered heart valves, *Biomaterials* 30 (2009) 4078–4084, <http://dx.doi.org/10.1016/j.biomaterials.2009.04.027>.
- [30] A. Atala, Tissue engineering of human bladder, *Br. Med. Bull.* 97 (2011) 81–104, <http://dx.doi.org/10.1093/bmb/ldr003>.
- [31] Y. Nagai, H. Yokoi, K. Kaihara, K. Naruse, The mechanical stimulation of cells in 3D culture within a self-assembling peptide hydrogel, *Biomaterials* 33 (2012) 1044–1051, <http://dx.doi.org/10.1016/j.biomaterials.2011.10.049>.
- [32] A. Mihic, J. Li, Y. Miyagi, M. Gagliardi, S.-H. Li, J. Zu, et al., The effect of cyclic stretch on maturation and 3D tissue formation of human embryonic stem cell-derived cardiomyocytes, *Biomaterials* 35 (2014) 2798–2808, <http://dx.doi.org/10.1016/j.biomaterials.2013.12.052>.
- [33] B.D. Fairbanks, M.P. Schwartz, A.E. Halevi, C.R. Nuttelman, C.N. Bowman, K.S. Anseth, A versatile synthetic extracellular matrix mimic via thiol-norbornene photopolymerization, *Adv. Mater.* 21 (2009) 5005–5010, <http://dx.doi.org/10.1002/adma.200901808>.
- [34] B. Riehl, J. Park, Mechanical stretching for tissue engineering: two-dimensional and three-dimensional constructs, *Tissue Eng. Part B* 18 (2012) 288–300, <http://dx.doi.org/10.1089/ten.teb.2011.0465>.
- [35] G. Huang, L. Wang, S. Wang, Y. Han, J. Wu, Q. Zhang, et al., Engineering three-dimensional cell mechanical microenvironment with hydrogels, *Biofabrication* 4 (2012) 042001, <http://dx.doi.org/10.1088/1758-5082/4/4/042001>.
- [36] C.E. Hoyle, T.Y. Lee, T. Roper, Thiol-enes: chemistry of the past with promise for the future, *J. Polym. Sci., Part A: Polym. Chem.* 42 (2004) 5301–5338, <http://dx.doi.org/10.1002/pola.20366>.
- [37] H. Liu, Q. Tan, W.R. Geddie, M.A.S. Jewett, N. Phillips, D. Ke, et al., Biophysical characterization of bladder cancer cells with different metastatic potential, *Cell Biochem. Biophys.* 68 (2014) 241–246, <http://dx.doi.org/10.1007/s12013-013-9702-9>.
- [38] J.J. Tomasek, G. Gabbiani, B. Hinz, C. Chaponnier, R.A. Brown, Myofibroblasts and mechano-regulation of connective tissue remodelling, *Nat. Rev. Mol. Cell Biol.* 3 (2002) 349–363, <http://dx.doi.org/10.1038/nrm809>.
- [39] H. Liu, J. Wen, Y. Xiao, J. Liu, S. Hopyan, M. Radisic, et al., In situ mechanical characterization of the cell nucleus by atomic force microscopy, *ACS Nano* 8 (2014) 3821–3828, <http://dx.doi.org/10.1021/nn500553z>.
- [40] J.D. McCall, K.S. Anseth, Thiol-ene photopolymerizations provide a facile method to encapsulate proteins and maintain their bioactivity, *Biomacromolecules* 13 (2012) 2410–2417, <http://dx.doi.org/10.1021/bm300671s>.
- [41] T.D. Hansen, J.T. Koepsel, N.N. Le, E.H. Nguyen, S. Zorn, M. Parlato, et al., Biomaterial arrays with defined adhesion ligand densities and matrix stiffness identify distinct phenotypes for tumorigenic and non-tumorigenic human mesenchymal cell types, *Biomater. Sci.* 2 (2014) 745, <http://dx.doi.org/10.1039/c3bm60278h>.
- [42] B.V. Sridhar, J.L. Brock, J.S. Silver, J.L. Leight, M.A. Randolph, K.S. Anseth, Development of a cellularly degradable PEG hydrogel to promote articular cartilage extracellular matrix deposition, *Adv. Healthcare Mater.* (2015), <http://dx.doi.org/10.1002/adhm.201400695>.
- [43] G. Sui, J. Wang, C.C. Lee, W. Lu, S.P. Lee, J.V. Leyton, et al., Solution-phase surface modification in intact poly(dimethylsiloxane) microfluidic channels, *Anal. Chem.* 78 (2006) 5543–5551, <http://dx.doi.org/10.1021/ac060605z>.
- [44] H.-Y.S. Huang, J. Liao, M.S. Sacks, In-situ deformation of the aortic valve interstitial cell nucleus under diastolic loading, *J. Biomech. Eng.* 129 (2007) 880–889, <http://dx.doi.org/10.1115/1.2801670>.
- [45] J.A. Kluge, G.G. Leisk, R.D. Cardwell, A.P. Fernandes, M. House, A. Ward, et al., Bioreactor system using noninvasive imaging and mechanical stretch for biomaterial screening, *Ann. Biomed. Eng.* 39 (2011) 1390–1402, <http://dx.doi.org/10.1007/s10439-010-0243-8>.
- [46] R.D. Cardwell, J.A. Kluge, P.A. Thayer, S.A. Guelcher, L.A. Dahlgren, D.L. Kaplan, et al., Static and cyclic mechanical loading of mesenchymal stem cells on elastomeric, electrospun polyurethane meshes, *J. Biomech. Eng.* 137 (2015) 1–8, <http://dx.doi.org/10.1115/1.4030404>.
- [47] T.M. Maul, D.W. Chew, A. Nieponice, D.A. Vorp, Mechanical stimuli differentially control stem cell behavior: morphology, proliferation, and differentiation, *Biomech. Model. Mechanobiol.* 10 (2011) 939–953, <http://dx.doi.org/10.1007/s10237-010-0285-8>.
- [48] Y. Cui, F.M. Hameed, B. Yang, K. Lee, C.Q. Pan, S. Park, et al., Cyclic stretching of soft substrates induces spreading and growth, *Nat. Commun.* 6 (2015) 6333, <http://dx.doi.org/10.1038/ncomms7333>.
- [49] E.D. O'Carbhaill, M.A. Punched, M. Murphy, F.P. Barry, P.E. McHugh, V. Barron, Response of mesenchymal stem cells to the biomechanical environment of the endothelium on a flexible tubular silicone substrate, *Biomaterials* 29 (2008) 1610–1619, <http://dx.doi.org/10.1016/j.biomaterials.2007.11.042>.
- [50] A.M. Quinlan, L.N. Sierad, A.K. Capulli, L.E. Firstenberg, K.L. Billiar, Combining dynamic stretch and tunable stiffness to probe cell mechanobiology in vitro, *PLoS ONE* 6 (2011), <http://dx.doi.org/10.1371/journal.pone.0023272>.
- [51] R.G. Ireland, C.A. Simmons, Human pluripotent stem cell mechanobiology: manipulating the biophysical microenvironment for regenerative medicine and tissue engineering applications, *Stem Cells* (2015). revision under review.